INTERNATIONAL JOURNAL OF ADVANCED STUDIES
IN COMPUTER SCIENCE & ENGINEERING
IJASCSE VOLUME 11 ISSUE 9 2022
09/30/2022

Fuzzy-PI Based Sliding Mode Control to Management of Hybrid Energy System Grid Connected

[1] M. Boukhalfa , [1]A. Benaissa , [2]A. A. Bengharbi , [3]M. R. Bengourina , [1]A. Khoudiri
[1]LAADI Laboratory, Faculty of Science and Technology, University of Djelfa , Algeria.
[2] Energy Engineering and Computer Engineering (L2GEGI) Laboratory, University of Tiaret, BP P 78 Zaâroura, 14000, Tiaret, Algeria.
[3]Centre de Développement des Energies Renouvelables, Algiers, Algeria.
*Corresponding Author Email: med.boukhalfa18@gmail.com

Abstract– This paper presents an optimized advanced control technique for a grid-connected hybrid energy system (HES) based on a solid oxide fuel cell (SOFC) and a photovoltaic panel (PV) in a distributed power generation system. A classical full sliding mode control and a Fuzzy-PI sliding mode are proposed for a system operation and power management mode (UPC mode). The latter technique which is based on a combination of a classical controller and fuzzy artificial intelligence system is utilized at power and current adjustment stage. The fuzzy system gave the optimal gain values to the PI controller to get a better performance. The obtained results show that the optimized sliding mode control (Fuzzy-PI) is better than the classical sliding one in terms of power, response time, and robustness against disturbances in production and consumption energy.

Keywords: Hybrid Energetic Systems; Solid Oxide Fuel Cell (SOFC); Photovoltaic Panel (PV) ; Sliding Mode Control; Fuzzy-PI control; Electrical Grid.

1. Introduction

In recent years, renewable energy sources have received increasing attention in order to solve the problems caused by the depletion of fossil fuels, mitigate the effects of climate change, and control global energy growth. Therefore, to face these problems, the members of 'Cop21' have proposed to invest more in renewable energies to produce electricity from photovoltaic panels, wind energy or solid oxide fuel cells (SOFCs). In fact, these sources are eco-friendly and more cost effective over time. However, it is not clear of lacks. For example, the electricity production from photovoltaic panels is not available all time [1-4]. To overcome this shortcoming, hybrid systems can be very useful.
A hybrid power system which is a mixture of two or more sources can be regarded as an alternative solution used together to provide better system efficiency as well as a better balance of renewable energy supplies [5]. Hybrid Energy systems (HESs) are currently growing due to the need to provide a continuous clean and reliable power supply; since the the fuel cell (SOFC) generates a direct current when the fuel (hydrogen and oxygen) is available, with a better efficiency about (60%) compared to the normal batteries. Thus, by varying the power output of the fuel cell, the output of the hybrid source can controlled [6]. Two types of hybrid systems are reported in literature according to their mode of interconnection to the network [7-10]: the autonomous hybrid systems and the distributed hybrid systems. Note that, generally, the distributed SRHs do not need storage system since the deficit and surplus between intermittent production and energy demand are compensated by the conventional electricity network. However, for the stand-alone SHERs, storage devices are needed to store the energy excess that can be re-injected later to meet the demand in case of energy deficit. The storage is also necessary if we wants to limit the power to be exchanged with the network.

2. Controller modeling and design

The adopted hybrid energy system (HES) uses the FC and the PV units represented in Figure. 1 as main power sources with a variable AC load. These distributed generation units are connected to the grid via two conversion modes DC/DC and DC/AC. The converters have then a three level NPC as VSI interface module with a series of an inductance line, considered as a filter to reduce the generated harmonics. The contained voltage bus side is kept constant by an appropriate control of each boost converter. The HES controller is designed for the FC/PV converters to satisfy the contained bus link power demand. The real and reactive powers are decoupled into the currents reference in the (*d-q*) axis in the "reference current calculation" block, and then controlled by the proposed "sliding mode controller" to generate the appropriate reference voltages to control the three-level inverter. This last step is performed using a three-level spatial

SVPWM modulation. The phase-locked loop (PLL) is used to synchronize the frequency and phase of the system with the main grid [11,12].

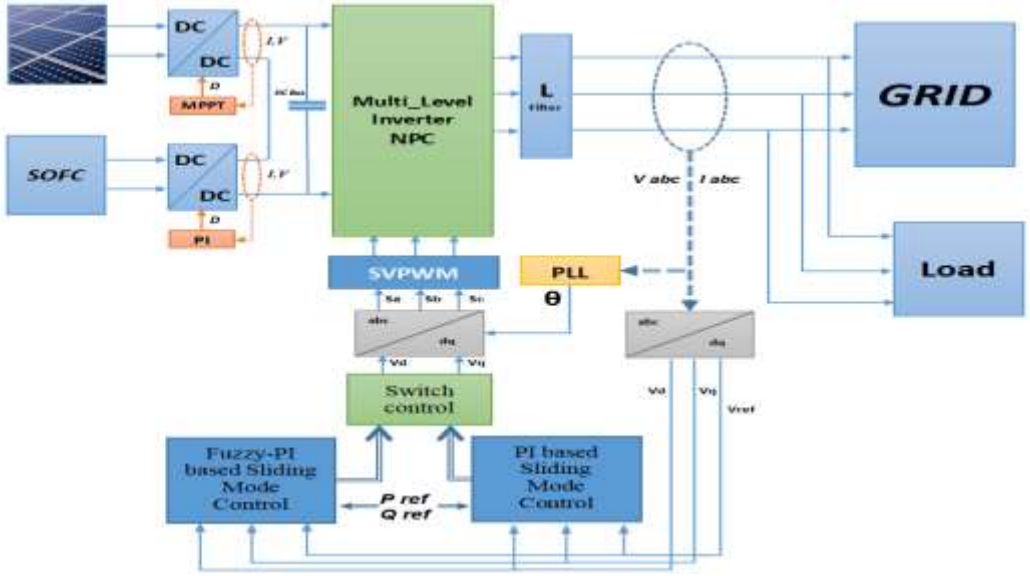

Figure 1. System overview of the PV/FC hybrid energetic system.

2.1. Modeling of the Solid oxide fuel cell (SOFC)

Solid oxide fuel cells (SOFCs) are widely used in energy production. They operate at very high temperatures (about 800 to 1000 °C). Their conversion efficiency can attain more than 60% [13,14].

The following assumptions considered :

- The fuel cell temperature is assumed to be constant.
- The fuel cell gasses are ideal.

According to Nernst's equation, the DC voltage V_{fc} across the stack of the fuel cell is given by :

$$V_{fc} = N_0[E_0 + \frac{R.T}{2.F}\ln\left(\frac{P_{H2}.P_{02}}{P_{H20}}\right)^{0.5})] - rI_{fc} \quad (1)$$

Where:

E_0: standard reversible cell potential (V).
P_i: partial pressure of species (Pa), (i: hydrogen, oxygen).
r: internal resistance of stack (Ω).
I_f : stack current (A).
N_0: number of cells in stack.
R: universal gas constant (R=8.314 J/mol K).
T: stack temperature (K).
F: Faraday's constant (C/mol).

The main equations describing the slow dynamics of a SOFC can be written as :

$$P_{ref} = V_{ref}.I_{ref} \quad (2)$$

$$\frac{dI_{fc}}{dt} = \frac{1}{T_e}[-I_{fc} + I_{ref}] \quad (3)$$

$$\frac{dq_{H2}^{in}}{dt} = \frac{1}{T_f}[\frac{dq_{H2}^{in}}{dt} - q_{H2}^{in} + \frac{2.K_r}{U_{opt}}.I_{fc}] \quad (4)$$

$$\frac{dP_{H2}}{dt} = \frac{1\frac{dP_{H2}}{dt}}{\tau_{H2}}[-P_{H2} + \frac{1}{K_{H2}}[q_{H2}^{in} - 2.K_rI_{fc}]] \quad (5)$$

$$\frac{dP_{02}}{dt} = \frac{1}{\tau_{02}}[-P_{02} + \frac{1}{K_{02}}.[\frac{1}{r_{H0}}.q_{H2}^{in} - 2.K_rI_{fc}\ ]] \quad (6)$$

$$\frac{dP_{H20}}{dt} = \frac{1}{\tau_{H20}}[\ -P_{H20} + \frac{2.K_r}{K_{H20}}.I_{fc}] \quad (7)$$

Where:

q_{H2}: Fuel flow (Mol/s).
q_{O2} : Oxygen flow (Mol/s).
K_{H2}: Valve molar constant for hydrogen (Kmol/s atm).
K_{O2}:Valve molar constant for Oxygen (Kmol/s atm).
K_{H2O}: Valve molar constant for Water (Kmol/s atm).
τ_{H2}: Response time for hydrogen (s).
τ_{02}: Response time for Oxygen (s).
τ_{H20}: Response time for water (s).
U_{H2O} : Optimum fuel utilization.
r_{HO}: Ratio of hydrogen to oxygen.
K_r : Constant (Kmol/s.A).
P_{ref}: Reference power (kW).

2.2. Photovoltaic model

The mathematical relation between current and voltage in the PV's single diode equivalent circuit is given by [15]:

$$I = I_{ph} - I_S\left[e^{\frac{q.(V.I.R_S)}{A.K.T}} - 1\right] - \frac{V.I+R_S}{R_{SH}} \quad (8)$$

$$I = N_P I_{Ph} - N_P I_S \left[e^{\left(\frac{Pq}{A.R.T}\right).\left(\frac{V}{N_S}+\frac{I.R_S}{N_P}\right)} - 1 \right] - \frac{N_P}{R_{SH}}\left(\frac{V}{N_S} + \frac{I.R_S}{N_P}\right) \quad (9)$$

Where:
I_{ph} is the photo-current source.
I_s: is the saturation currents.
q: is the electron charge (1.602×10^{-19} C).
K : is the Boltzmann constant (1.381×10^{-23}).
T: is the cell temperature.
A: is the junction ideality factor.
N_s: is the numbers of the series cells.
N_p: is the parallel cells.
R_s: the internal losses resistance.
R_{sh}: the internal shunt resistance in parallel with a diode to take into account the leakage current to the ground.
The photo-current depends on the solar radiation and the cell temperature [16,17] and is written as :

$$I_{ph} = \left(\frac{S}{S_{ref}}\right)[I_{ph,ref} + C_T(T - T_{ref})] \quad (10)$$

Where:
S : is the real solar radiation (W/m^2).
S_{ref}, T_{ref}: are respectively solar radiation and temperature.
C_T: is the temperature coefficient (A/K). [18].

The saturation current Is varies with the cell temperature as:

$$I_S = I_{S,ref}\left(\frac{T}{T_{ref}}\right)^3 e^{\left[\frac{q.E_g}{A.K}.\left(\frac{1}{T_{ref}}-\frac{1}{T}\right)\right]} \quad (11)$$

Where:
I_{sref} is the saturation current in standard test conditions.
E_g : is the band-gap of the cell semi-conductor (eV) depending on the cell material.

2.3. Maximum power point tracking (MPPT) control method

The P&O (MPPT) algorithm shown in Figure. 2 is the most widely used method since it is simplicity and performing well in changing atmospheric conditions [18-20].

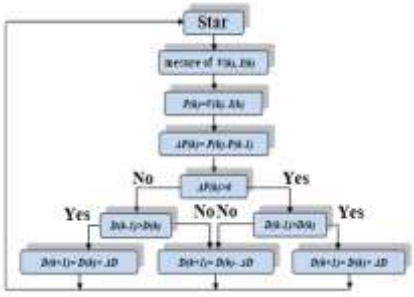

Figure 2. The P&O (MPPT) algorithm

2.4. Modeling of DC-DC Boost converter

In the studied PV-FC hybrid power system shown in Figure. 1, there are two boost converters used; in the case of a PV source, it is used to extract the maximum power using the MPPT algorithm, and for the SOFC source, the boost converter is used to obtain the required fixed DC voltage using a simple PI controller. The average state space model of the converter is given by:

$$\dot{X} = X(t) + BX(t) \quad (12)$$

Where:

$X(t) = [i_L . V_c]^T$ is the state vector, A and B: are the system matrices:

$$A = \begin{bmatrix} \frac{-1}{C(R+r_c)} & \frac{R(1-D)}{c(R+r_c)} \\ \frac{R(1-D)}{c(R+r_c)} & \frac{-1}{L}\left(r_L + \frac{Rr_c}{r_c}\right) \end{bmatrix}, \quad B = \begin{bmatrix} 0 \\ \frac{1}{L} \end{bmatrix}$$

Where:
r_L and r_c: are the internal series resistors of the inductor and capacitor; D: is the switching duty-ratio.

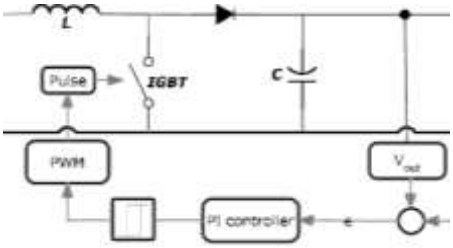

Figure 3: Boost converter circuit [23] [24]

2.5. Modeling and control of the three levels NPC inverter

The three-level NPC inverter in the HES system allows reducing the high order harmonics leaded by PMW modulation [21]. As shown in Figure. 4 the equivalent circuit of the NPC inverter contains a voltage source inverter and a clamped diode converter based on the clamped neutral point (CNP). These are more attractive for medium and high voltage applications (like reactive power compensation, active power filters). They have also the advantages for blocking the voltage of switching device which is a half of the DC voltage. The output harmonics are much lower than that of a two-level inverter at the same frequency of switching [22].

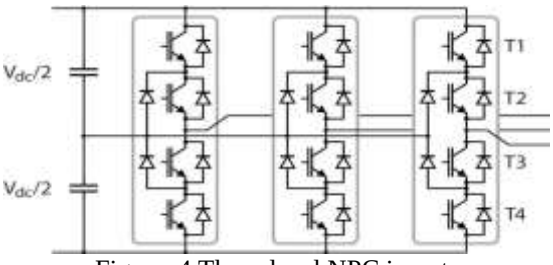

Figure. 4 Three-level NPC inverter

The model of the NPC-VSI is carried out under the following assumptions:

- The AC voltage is a balanced three-phase system.
- All circuit elements are LTI (Linear Time Invariant).
- The power switches are ideal.

The AC side is a matrix form with the following mathematical model [25]:

$$\frac{d}{dt}\begin{bmatrix} i_d \\ i_q \\ i_c \end{bmatrix} = \begin{bmatrix} -\frac{R}{L} & 0 & 0 \\ 0 & -\frac{R}{L} & 0 \\ 0 & 0 & -\frac{R}{L} \end{bmatrix}\begin{bmatrix} i_d \\ i_q \\ i_c \end{bmatrix} + \frac{1}{L}\begin{bmatrix} V_{ga}-e_c \\ V_{gb}-e_q \\ V_{gc}-e_c \end{bmatrix} \quad (13)$$

The filter has an inductance L and an internal resistance R. V_{gi} : is the main grid AC voltage, i (i=a, b, c).The inverter voltage in the DC side currents are given by:

$$I_{c0} = I_{c1} + I_{c2} \quad (14)$$

The DC side capacitor voltages is given by:

$$\frac{d}{dt}\begin{bmatrix} U_{c1} \\ U_{c2} \end{bmatrix} = \frac{d}{dt}\begin{bmatrix} I_{c1} \\ I_{c2} \end{bmatrix} \quad (15)$$

Thus, in the balanced condition we can put :

$$I = I_{c1} = I_{c2} \text{ and } U = U_{c1} = U_{c2} \quad (16)$$

Finally, the output active and reactive power of the three level inverter can be given by:

$$P_g = V_{ga}i_{ga} + V_{gb}i_{gb} + i_{ga} + V_{gca}.i_{gc} \quad (17)$$

$$Q_g = \frac{1}{\sqrt{3}}(V_{gab}\, i_{gc} + V_{gbc}i_{ga} + V_{gca}i_{gb}) \quad (18)$$

Where:
V_{ga}, V_{gb} and V_{gc}: are the three-phase voltages at the AC bus.
I_{ga} ,I_{gb}, and I_{gc}: are the three-phase currents injected into the AC grid.

2.5.1. Model of the three level inverter in the (*dq*) frame

As part of the control strategy, Park's transformation is used to transfer the coordinates from the stationary three-phase system (*a*,*b*,*c*) to the rotating coordinate system (*dq*) which rotates with a frequency ω using the information from a three-phase PLL as illustrated in Figure. 5.

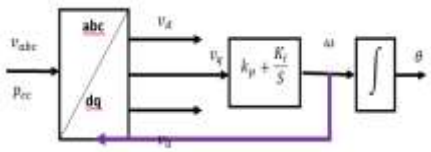

Figure 5. Schematic diagram of the phase locked loop (PLL)

The transformation matrix *Ks* is given by:

$$\begin{bmatrix} cos(wt) & \cos(wt-\frac{2\pi}{3}) & cos(wt+\frac{2\pi}{3}) \\ sin(wt) & sin(wt-\frac{2\pi}{3}) & \sin(wt+\frac{2\pi}{3}) \\ 1/2 & 1/2 & 1/2 \end{bmatrix} \quad (19)$$

Applying Park's transformation, the state space model of the three-level NPC converter in the (*dq*) frame becomes:

$$\frac{d}{dt}\begin{bmatrix} i_d \\ i_q \\ V_{dc} \end{bmatrix} = \begin{bmatrix} -\frac{R}{L} & w & 0 \\ -w & -\frac{R}{L} & 0 \\ 0 & 0 & 0 \end{bmatrix}\begin{bmatrix} i_d \\ i_q \\ V_{dc} \end{bmatrix} + \begin{bmatrix} \frac{1}{L} & 0 & 0 \\ 0 & \frac{1}{L} & 0 \\ 0 & 0 & \frac{1}{C_{eq}} \end{bmatrix}\begin{bmatrix} V_d \\ V_q \\ i_{dc} \end{bmatrix} + \begin{bmatrix} -\frac{1}{L}V_{gd} \\ -\frac{1}{L}V_{gq} \\ 0 \end{bmatrix} \quad (20)$$

Where:
V_{gd} ,V_{qq} are the (*dq*) axis components of the main grid voltages.
i_d , i_q: are the line currents.
V_d , V_q: are the converter output voltages.
C_{eq}= C/2 is the DC-link equivalent capacitor.
V_{dc} : is the DC bus voltage.
I_{dc} : is the equivalent DC current.

The dynamic DC equivalent voltage V_{dc} is derived using the equation :

$$i_{dc} = C_{eq}\frac{d}{dt}V_{dc} \quad (21)$$

The apparent power is given by :

$$\bar{s}=p_s + jq_s \quad (22)$$

Where Ps and qs are the active and reactive powers produced by the system.
In our case, the instantaneous active and reactive powers which are supplied to the network line in the frame of rotation (*dq*) are given by [26-28] :

$$P_s(t)=\frac{3}{2}(V_{sd}(t).i_d(t)+ V_{sq}(t).i_q(t)) \quad (23)$$

$$Q_s(t)=\frac{3}{2}(-V_{sd}(t).i_q(t)+V_{sq}(t).i_d(t)) \quad (24)$$

In the reference frame synchronized with the grid voltage, we assume that V_{gq}=0, V_{gd} =V_g , then:

$$P_s(t)=\frac{3}{2}(V_{gd}(t).i_d(t) \quad (25)$$

$$Q_s(t)=\frac{3}{2}(-V_{gq}(t).i_q(t)) \quad (26)$$

2.5.2. Control strategy

The proposed control strategy of the three level NPC inverter and the power system based on the use of a discreet time integral sliding mode controller [26,29].
The system given in equation (20) has the form:

$$\dot{X} = AX + BU + C \quad (27)$$

With:

$X=[i_d, i_q, V_{dc}]^T$ and $U=[V_d, V_q, I_{dc}]^T$

Then:

$$A=\begin{bmatrix} -\frac{R}{L} & w & 0 \\ -w & -\frac{R}{L} & 0 \\ 0 & 0 & 0 \end{bmatrix}, B=\begin{bmatrix} \frac{1}{L} & 0 & 0 \\ 0 & \frac{1}{L} & 0 \\ 0 & 0 & \frac{1}{C_{eq}} \end{bmatrix}, C=\begin{bmatrix} -\frac{1}{L}V_{gd} \\ -\frac{1}{L}V_{gq} \\ 0 \end{bmatrix}$$

Firstly, we consider the following three new variables:

$X_1=(i_d-i_{dref})$, $X_2=(i_q-i_{qref})$, $X_3=(V_{dc}-V_{dref})$.

The reference currents (i_{dref}, i_{qref}) are related to the reference active and reactive powers in the plane (dq) by the following equations:

$$\begin{cases} P_{rg} = 3/2(V_{ref} I_{dref}) \\ Q_{rg} = 3/2(-V_{ref} I_{qref}) \end{cases} \quad (28)$$

Then:

$$\begin{cases} I_{dref} = 2/3(P_{ref}/V_{ref}) \\ Q_{rg} = -2/3(Q_{ref}/V_{ref}) \end{cases} \quad (29)$$

Note that V_{dr}: is fixed by the grid-connected system designer [30].

By taking the transpose matrix $X=[X_1,X_2, X_3]^T$ the system (27) can be rewritten as:

$$\dot{X} = AX + BU + D \quad (30)$$

With:

$$D=C+A\left[i_{dref}, i_{qref}, V_{dcref}\right]^T \quad (31)$$

For discrete time, the model in equation (30) becomes:

$$X(k+1)= A_d X(k) + B_d U(k)+D_d \quad (32)$$

where: A_d, B_d and D_d are the discrete time matrices obtained using a blocking order of zero order to the system (30).

The proposed control strategy of the three-level inverter is based on the use of an integral sliding mode controller (SMC) in discrete time. The objective of this command is to force the system state to reach in a finite time and stay in a slippery surface σ (x) = 0 with a controlled and stable dynamic behavior.

The sliding surface adopted is chosen to have both proportional and integral actions. In discrete time, this surface is given by:

$$\sigma(k)=K_p X(k) +K_i T_s \sum_{j=0}^{k-1} X(j) \quad (33)$$

where: K_p and K_i are the controller parameter matrices per SMC; and (k = 0,1,2,...).

An adequate choice of (K_p , K_i) ensures that the system remains in the sliding surface which is defined by:

$$\sigma(k)= 0 \quad (34)$$

Furthermore,

$$\sigma(k+1) = k_p x(k+1) + k_i T_s \sum_{j=0}^{k} x(j) \quad (35)$$

Thus:

$$\sigma(k+1) = \sigma(k) + k_p x(k+1) + \left(k_i T_s - k_p\right) x(k) = 0 \quad (36)$$

Where:

$$x(k+1) = \left(I - k_p^{-1} k_i T_s\right) x(k) \quad (37)$$

This means that the system state will depend only on the choice of controller parameters.

The proposed controller in discrete time has the following form:

$$\begin{cases} U(k+1) = U_{eq}(k) + U_{NL}(k) \\ U_{eq}(k+1) = f(U(k)) \end{cases} \quad (38)$$

with: U_{eq} (k+1) is the equivalent command and $U_{NL}(k)$ is the non-linear command.

The nonlinear command is added as follows:

$$U_{NL}(k) = N sign(\sigma(k)) \quad (39)$$

where: N is a matrix with non-negative constant elements.

Hence, the SMC controller is :

$$U(k) = -\left(k_p B_d\right)^{-1}\left[k_p(A_d - I) + K_i T_S\right]\left[A_d X(K-1) + B_d U_{eq}(K-1) + D_d\right] + K_p D_d + \sigma(k)+N.sign(\sigma(k) \quad (40)$$

Finally, the reference signals ($V_d(k)$,$V_q(k)$) are modulated using the three-level vector modeling (SVPWM) to give states to the inverter switches.

2.5.3 Three-level space vector modulation

This section presents the three-level NPC inverter space vector modultation (SVM) topology, the output voltages can be presented in the space on an ($\alpha\beta$) plane corresponding to the switching states of the inverter. Basing on their magnitudes, the 19 space vectors correspond to the 27 switching states of the three-level NPC inverter and the projection of the vectors on ($\alpha\beta$) coordinates forms a two-layer hexagon centered at the origin of the ($\alpha\beta$) plane as figured in Figure. 6 and zero voltage vectors are located at the origin of the plane. The switching states are illustrated by 0,1 and 2, which denote the corresponding switching states [31]. The reference voltage vector V_{ref} is the geometric sum of the three vectors (V_1, V_2, V_3) chosen multiplied by their switch on duration (d_1, d_2, d_3). The sum of their switch on duration must be equal to the complete cycle T. The switching orders of the inverter switches can be determined numerically or analytically through mathematical equations:

$$v_1 d_{1+} v_2 d_{2+} v_3 d_3 = v_{ref} T \quad (41)$$

$$d_3 + d_2 + d_3 = T \quad (42)$$

$$\left\|v_{ref}\right\| e^{j\theta} = v_{ref} \quad (43)$$

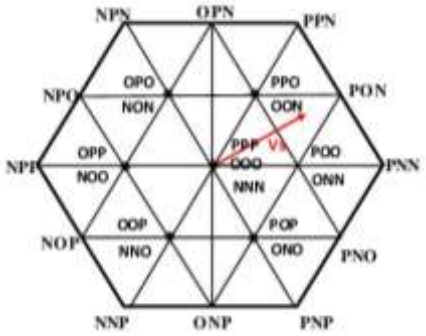

Figure. 6 Space vector diagrams of a multilevel inverter [32]

3. Power management strategy

An optimized management plan of a hybrid energy system is proposed. It operates as follows:

- a fixed stable power output from the hybrid system, which can be changed according to the grid demand and independently of the local load demand is assumed.
- If the power produced by the PV-FC systems is adjusted independently to the local load demand, then the system operates in unit power control mode (UPC mode).
- The SOFC acts as a secondary source to meet the demand and ensure a stable and better quality power output even in poor weather or dark conditions.
- If the local load power demand is less than the reference power produced by the PV-FC system, the excess power produced will be injected into the grid.
- If the load power demand is greater than that generated by the PV-FC system of the SEH, the power shortfall to the load demand will be provided by the grid.

To reach this objective, we will present in the following section the integral sliding mode and fuzzy-PI sliding mode control techniques, applied to the multilevel NPC inverter. Then comparing the results obtained of both techniques.

4. Results and simulations

4.1. Simulation of the SEH system under variable weather conditions

Simulations of the different parts of the system are developed in Matlab/Simulink allowing to compare the performance of the two PI-based sliding control modes and the Fuzzy-PI based sliding mode control, for our studied hybrid energy system. In this case, the power produced by the SEH is independent of the load. As a reference we consider a jump in active power from 150 kW to 100 kW at t = 2s and zero reactive power. On the other hand, the weather conditions are variable as shown in Figures (12) and (13). The PV panel is controlled using the MPPT algorithm by (P&O-MPPT), so both power products (SOFC and PV) will vary together to supply the load. From the simulation results, it can be seen that the output voltage and current of the SOFC in Figures (16) and (17) depend on the power of the GPV. In case of unfavorable weather conditions, they act so as to compensate the decrease in PV power generation in order to reach the fixed power in UPC mode as shown in Figure (14). The difference between the generated and consumed power will be injected into the grid (the negative power grid at t >2s). If the maximum generation limit is reached, the system will maintain its generation level and the remaining power to supply the load which will be generated by the grid. From the control viewpoint, the static error is negligible between the reference power and the output power of the hybrid system. Thanks to the SM controller, it can be noticed that the tracking produced by the fuzzy sliding mode with the presence of a PI controller is more accurate and smooth compared to that produced by the clasic sliding mode control, and the response time is faster in the transient regime of the sliding mode with fuzzy_PI controller compared to the sliding mode with PI controller. The variation of the load power and the system performance are negligible, moreover, the DC bus voltage is maintained at a constant value of 900 V according to Figure. 21 where each of the input capacitors of the NPC inverter is at almost half of this voltage. Furthermore, the use of the SVPWM for operation at a guaranteed fixed switching frequency improves the quality of the AC voltage where the grid voltage (L-L) is 400 V (figures (9),(11) and (18)) for all load and weather conditions. This validates the good behavior of the discrete-time fuzzy-integral controller (SMC) compared to the integral controller (CMC). The delay in the response is due to the time constant of the SOFC in the first place. The reactive power is also controlled independently of the load, where it is set to zero, and the required reactive power (Q=1000 VAR) is generated by the grid. According to our results, the two modes shows that the integral technique (SMC) despite it has the advantage to reduce the interference action, it possesses a non- inconvenient mathematical model requirement and causes the phase delay problem. The SMC fuzzy-pi technique has the ability to approximate any non-linear function with a given degree of accuracy.

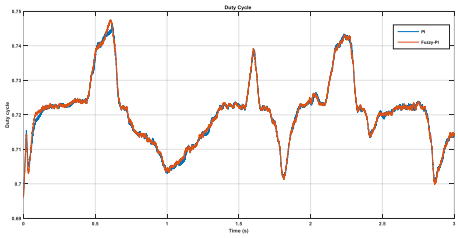

Figure. 7 Duty cycle (D) generated by P&O MPPT

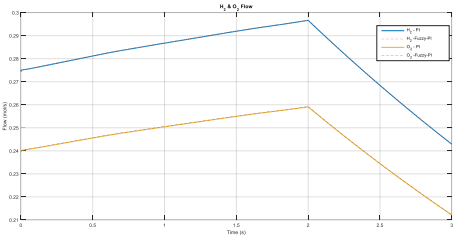

Figure. 8 Hydrogen, Oxygen flow

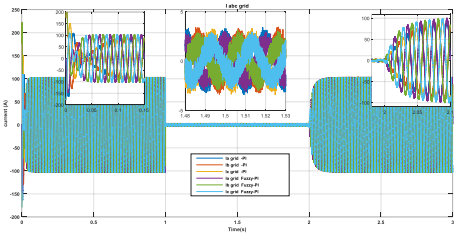

Figure. 9 Grid output currents (A)

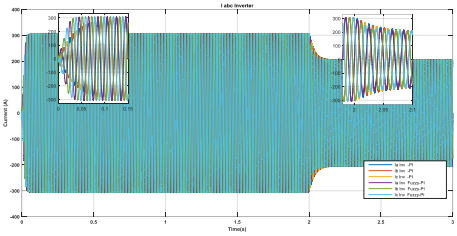

Figure. 10 Inverter output currents (A)

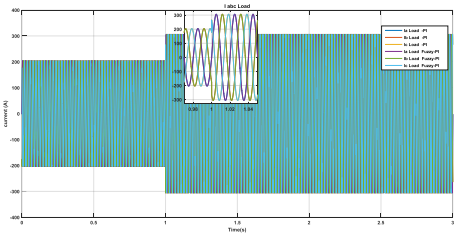

Figure. 11 Load output currents (A)

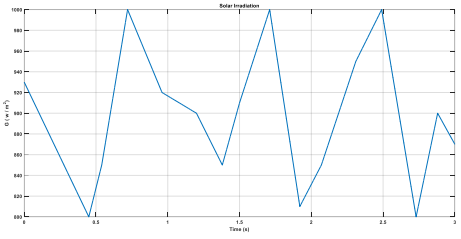

Figure. 12 Temperature profile

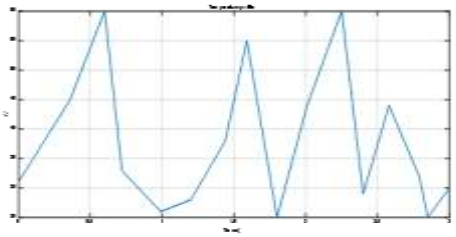

Figure. 13 Solar irradiation profile

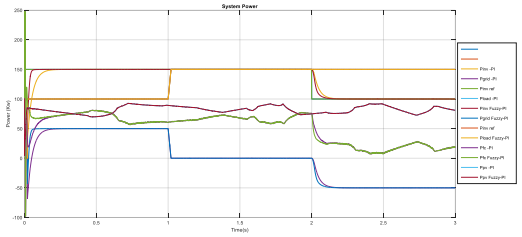

Figure. 14 System powers (kW)

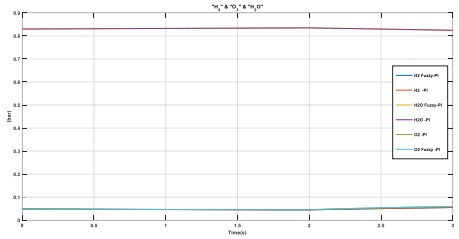

Figure. 15 Hydrogen, Oxygen and water pressures

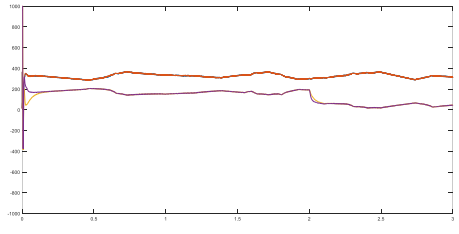

Figure. 16 PV and SOFC output currents (A)

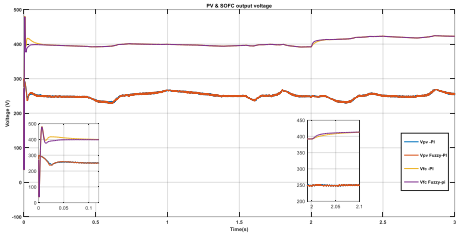

Figure. 17 PV and SOFC output voltages (V)

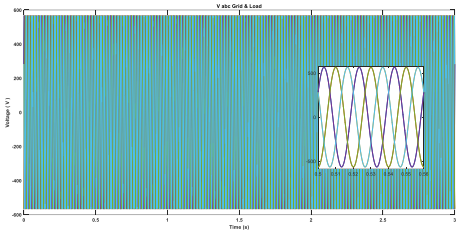

Figure. 18 voltage output grid and load

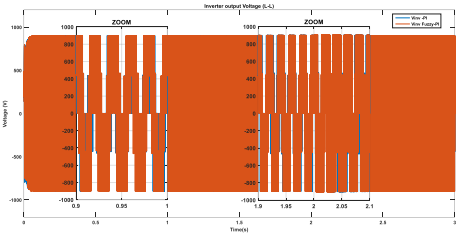

Figure. 19 inverter output voltage (L-L)

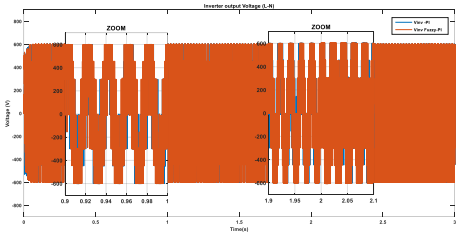

Figure. 20 inverter output voltage (L_N)

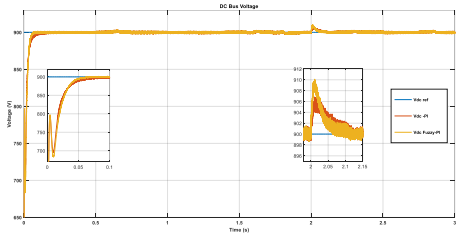

Figure. 21 DC_Bus Voltage

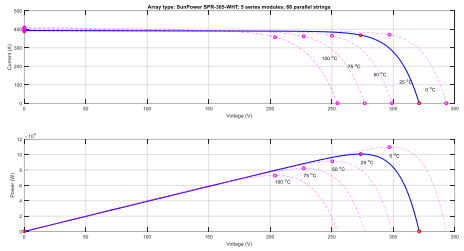

Figure. 22 Effect of temperature (T) on the I-V and P-V curve at 1000 W/m2.

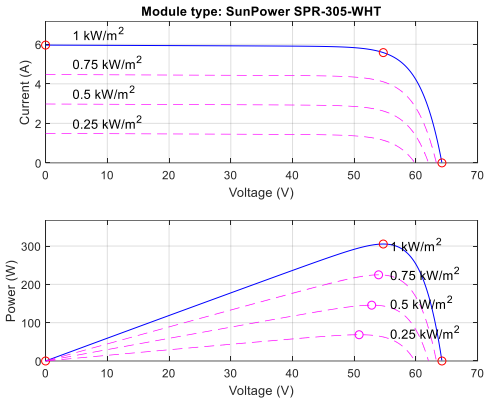

Figure. 23 Effect of irradiation on the I-V and P-V curve at 25°c

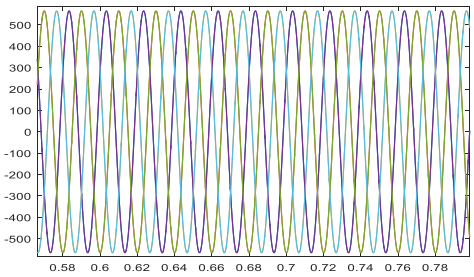

Figure. 24 Zoom voltage output grid and load

5. Conclusion

In this paper, a comparative study between sliding mode control based on conventional controllers and sliding mode control based on fuzzy PI, in a grid-connected SEH hybrid electric system without battery storage is presented. The SEH hybrid power system consists of a SOFC fuel cell, a GPV and a variable AC load. The GPV is connected via a boost controlled by a P&O and MPPT. The GPV is connected to a boost chopper controlled by a PI controller and the GPV/SOFC is connected to a multilevel inverter NPC connected to the grid controlled by SVPWM, which maintains the proposed control signals that allows the power management of the system from the determination of the controller gains using a tabular fuzzy logic and

the obtaining of an AC voltage at the output of a multilevel inverter of better quality, to ensure an optimal performance of the proposed system power flow. The main objective of this work is to improve and optimize the proposed controller from the gain determination by using tabular fuzzy logic table to ensure an optimal power flow performance of the proposed system.

The future scope

The results of our work have allowed us to draw the following perspectives:

- Adding a fast storage system (super capacitor) and increasing the advantage of the autonomy of the system, thus eliminating the need for the network in transient regime.
- It would be important to change the optimized control by a real time adaptation algorithm (adaptive sliding mode) and test the dynamic performance on a real system.

Appendix

A. Parameters values of photovoltaic array (at 250C) are given as bellow

Var.	Representation	Values
f_s	Frequency	5.4 khz
L	Inductance	4mH
R_1	Resistance	0.01 Ω
C	capacitor	2000 uf
r_c	Resistance	0.01 Ω

B. Parameters of DC-DC Boost converter (connected to PV)

Var.	Representation	Values
f_s	Frequency	5.4 khz
L	Inductance	5mH
R_1	Resistance	0.01 Ω
C	capacitor	5000 uf
r_c	Resistance	0.1 Ω

C. Parameters of DC-DC Boost converter (connected to SOFC)

Var.	Representation	values
T	Absolute temperature	1273 K
F	Faraday's constant	96487 C/mol
R	Universal gas constant	8314 (J/ Kmo K)
E_0	Standard reversible cell potenti	1.18 V
N	Number of cells in stack	450
K_r	Constant	996*10-6 (Kmol/sA)
U_{max}	Maximum fuel utilization	0.9
U_{min}	Minimum fuel utilization	0.8
U_{opt}	Optimum fuel ratio	0.85
K_{H2}	Value molar constant for hydrogen	8.43*10-4 Kmol/(s atm)
Ko_2	Value molar constant for oxyge	2.81*10-4 Kmol/(s atm)
K_{H2o}	Value molar constant for water	2.52*10-3 Kmol/(s atm)
τ_{H2}	Response time for hydrogen fl	26.1 s
τ_{o2}	Response time for oxygen flow	2.91 s
τ_{H2o}	Response time for water flow	78.3 s
R	Ohmic loss	0.126 Ω
T_e	Electric response time	0.8 s
T_f	Fuel processor response time	0.03 s
r_{HO}	Ration of hydrogen to oxygen	1.145

D. Solid Oxide Fuel (SOFC) parameters

Var	Representation	Value
N_s	Numbers of the series modules	5
N_p	Numbers of the parallel modules	66
N_m	Numbers of the cells per module	96
V_{oc}	Open circuit voltage	64.2 V
I_{sc}	Short-circuit current	5.96 A
V_{mp}	Voltage at max. power point	54.7 V
I_{mp}	Current at maximum power point	5.58 A
Q_d	Diode Quality factor	1.25
I_{ph}	Photo-current source	5.96 A
I_{sat}	Diode saturation current	$5.26\ 10^{-19}$ A
R_p	Parallel resistance	819.3 Ω
R_s	Series resistance	0.083 Ω

References

[1] B. Multon et H. Ben Ahmed, « Le stockage stationnaire d'énergie électrique : pourquoi et comment », Revue 3E.I, n°48, pp. 18-29, mars 2007.

[2] D. Lu, « Conception et contrôle d'un générateur PV actif à stockage intégré Application à l'agrégation de producteurs-consommateurs dans le cadre d'un micro réseau intelligent urbain », thèse de doctorat, Ecole centrale de Lille, 2010.

[3] G. Cimuca, « Système inertiel de stockage d'énergie associé à des générateurs éoliens », thèse de doctorat, université de Lille, 2004.
[4] G. Cimuca, S. Breban, M. Radulescu, C. Saudemont, B. Robyns, « Design and control strategies of an induction machine based fywheel energy storage system associated to a variable speed wind generator. », Energy Convers IEEE Trans, 25:526–34, 2010.
[5] A. Helal, R. El-Mohr y H. Eldosouki, "Optimal Design of Hybrid Renewable Energy System for Electrification of a Remote Village in Egypt,"Arab Academy for Sciences & Technology and Maritime Transport Alexandria.
[6] S. Moussa, A. Kaabèche et M. Belhamel article Rev. Energ. Ren. : '' Evaluation des Performances d'un Système Hybride de Production d'Electricité - Fourniture d'énergie électrique sans interruption au moyen d'un système hybride (solaire, éolien, et diesel) totalement autonome '' Valorisation (1999) 247-250.
[7] A. Chih et C. Hua, « Charge and Discharge Characteristics of Lead-Acid Battery and LiFePO4 Battery », International Power Electronics Conference, 2010.
[8] S. A. Belfedhal, E.M. Berkouk, Y. Messlem, « Analysis of grid connected hybrid renewable energy system », Journal of Renewable and Sustainable Energy, doi.org/ 10.1063/ Janv 2019.
[9] BENGOURINA Mohamed Rida, "Commande avancée d'un filtre actif parallèle en utilisant une approche métaheuristique : application aux systèmes photovoltaïques interconnectes au reseau". these doctorat en science ,2020.
[10] S.J. Lee, J.K. Kang and S.K. Sul, 'A New Phase Detecting Method for Power Conversion Systems Considering Distorted Conditions in Power System', In Proceedings of Industry Applications Conference, 34 Annual Meeting, Vol. 4, 1999.
[11] S.M. Silva, L.N. Arruda, and B.J. Cardoso Filho, 'Wide Bandwidth Single and ThreePhase PLL Structures for Utility Connected Systems', In Proceedings of European Power Electronics, 2001.
[12] C. Zuo, M. Liu, M. Liu , "Solid Oxide Fuel Cells, Sol-Gel Processing for Conventional and Alternative Energy," Chapter 2, pp.7-36, Springer Science, 2012.
[13] S. Udroiu, ''Développement de Piles à Combustible de type SOFC en Technologie Planaire Couches Epaisses. Application à l'Etude de Dispositifs en Configuration Monochambre ''. Thèse de Doctorat Ecole Nationale Sup.des Mines de Saint-Étienne, 2009.
[14] S. Abdeslem, « Filtrage actif et contrôle de puissances: application aux systèmes photovoltaïques interconnectés au réseau ». Mémoire de magister université Ferhat Abbas – Sétif UFAS (Algérie) 2012.
[15] A. Goetzberger, V. Hoffman, U.Volker, "Photovoltaic Solar Energy Generation", Optical Sciences, Springer, 2005.
[16] I. Vechiu, " Modélisation et Analyse de l'Intégration des Energies Renouvelables dans un Réseau Autonome , " Thèse de doctorat, Université du Havre, 200.
[17] M. Sahnoun,"Contribution à la Modélisation et au Contrôle de trajectoire de Trackers Photovoltaïque à Haute Concentration (HCPV) ," Thèse de doctorat, Ecole Nationale Supérieur de l'Arts et Métiers, 2015.
[18] T. Esram , P. L. Chapman, "Comparison of Photovoltaic Array Maximum Power Point Tracking Techniques, " IEEE Trans. Energy Conversion v22 , No. 2, pp439-449. 2007.
[19] J G. Walker, " Evaluating MPPT Converter Topologies Using a Matlab PV Model, " Journal of Electrical & Electronics Engineering, v21, N°. 1, pp.49-56, Australia, 2001.
[20] Erickson, R.W., D. Maksimovic "Fundamentals of power electronics, Second edition, Kluwer Academic Publishers", New York(2001).
[21] Sezen, S., E. Özdemir (2013) Modeling, simulation and control of threephase three level multilevel inverter for grid connected photovoltaic system, Journal of optoelectronics and advanced materials 15(3-4): 335-341.
[22] I. Vechiu, " Modélisation et Analyse de l'Intégration des Energies Renouvelables dans un Réseau Autonome , " Thèse de doctorat, Université du Havre, 2005.
[23] M. Camara, B. Dakyo, H. Gualous, "Polynomial Control Method of DC/DC Converters for DCBus Voltage and Currents Management-Battery and Supercapacitors," IEEE Transactions on Power Electronics v27 , no. 3, 1455–1467, 2012.
[24] Portillo, R., S. Vazquez, J.I. Leon, M.M. Prats, L.G. Franquelo (2013) Model based adaptive direct power control for three-level npc converters, IEEE Transactions on industrial informatics 9(2): 1148-1157.
[25] Utkin, V., J. Gulder, J. Shi "sliding mode control in electromechanical systems", 1999.
[26] K.M. Arun Prasad, A. Unnikrishnan and N. Usha, 'Fuzzy Sliding Mode Control of a Switched Reluctance Motor', Global Colloquium in Recent Advancement and Effectual Researches in Engineering, Science and Technology, 'RAEREST', 2016.
[27] J. Hu , J. Zhu , D. G. Dorrell " Model Predictive Control of Grid Connected Inverters

for PV Systems with Flexible Power Regulation and Switching Frequency Reduction", IEEE Trans. Ind. Appl., v51, No.1, pp. 587–594, 2015

[28] Villalva, M. G., J.R. Gazoli, E.R. Filho (2009) Comprehensive approach to modeling and simulation of photovoltaic arrays, IEEE Transactions on power electronics 24 (5): 1198-1208.

[29] Sarpturk, S.Z., Y. Istefanopulos, O. Kaynak (1987) On the stability of discrete-time sliding mode control systems, IEEE Transaction on Automatic Control 32(10): 930-932.

[30] Ramírez, J. D.B., J.R. Rivas (2012) DSP-based simplified space-vector pwm for a three-level vsi with experimental validation, Journal of power electronics 12(2): 285-293.

[31] M.H. Rachid, "Power Electronics Handbook: Devices, Circuits and Applications," Third Edition, Elsevier's Science & Technology, ISBN: 978-0-12-382036-5, USA, 2011.